

**Chaotic function generator: Complex dynamics and its control in a loss-modulated Nd:YAG laser**R. Meucci,<sup>1</sup> Ryan McAllister,<sup>2,3,4</sup> and Rajarshi Roy<sup>2,3,4,5</sup><sup>1</sup>*Istituto Nazionale di Ottica Applicata, Largo Enrico Fermi, 6-50125 Firenze, Italy*<sup>2</sup>*Department of Physics, University of Maryland, College Park, Maryland 20742*<sup>3</sup>*IREAP, University of Maryland, College Park, Maryland 20742*<sup>4</sup>*CESAR, Computing and Computational Sciences Directorate, Oak Ridge National Laboratory, Oak Ridge, Tennessee 37831-6355*<sup>5</sup>*IPST, University of Maryland, College Park, Maryland 20742*

(Received 15 April 2002; published 27 August 2002)

The complex dynamics resulting from electronic feedback of a laser's intensity are explored and characterized. Distinct stable and chaotic regimes can be elicited from the laser by tuning the bias of the feedback loop. An additional branch of the feedback loop, containing a derivative filter, provides access to new kinds of dynamics, including a more gradual transition to chaos. The whole feedback network together allows the laser dynamics to be selected from among a wide range of chaotic wave forms distinguished by statistical or spectral information. In other words, this laser system can be used as a tunable generator of chaotic functions.

DOI: 10.1103/PhysRevE.66.026216

PACS number(s): 05.45.Gg, 95.10.Fh, 42.65.Sf

**I. INTRODUCTION**

There is continued growth in the field of nonlinear dynamics and an ever-increasing appreciation of its applications among researchers. With this growth, devices capable of generating complicated wave forms may be of use to complement the standard function generator. In this paper, we construct an example of such a device and present the concept of its operation.

We build a laser with externally accessible tuning parameters. Within a range of tuning, the laser exhibits a variety of dynamics, including low-dimensional chaos. As chaotic wave forms are not periodic functions, these dynamics are best distinguished from one another by their statistical characteristics. It is possible to create a table of the recorded statistical characteristics of the chaotic time series for different values of the tuning parameter(s). Once such a lookup table is built, the laser may be used to generate wave forms selected by the information recorded about them. In this paper, we will calculate and record the discrete probability density functions, the power spectra, and the leading Lyapunov exponents of the wave forms generated by the laser.

The time evolution of a generic homogeneously broadened laser is described by three dynamical variables: the complex electric field, the population inversion, and the complex polarization [1]. In a class-B laser, of which a neodymium laser is an example, the decay rate of the polarization is large enough compared to those of the other two variables, so that the polarization is essentially determined by the instantaneous values of the electric field and inversion [2]. Neodymium lasers, such as the one used here, are often employed for research and industrial applications in either stable [continuous wave (cw)] or regularly pulsed modes of operation [3].

There are simple ways to generate chaotic wave forms from lasers for uses such as transmitting digital information [4]. It may also be possible to generate wave forms appropriate for encoding speech. One method to induce these kinds of chaos in a laser is modulation with an external periodic signal.

A simple way to destabilize a class-B laser without an external drive is through the use of feedback. This configuration was proposed for the first time in 1986 for a CO<sub>2</sub> laser with an intracavity electro-optic modulator (EOM) [5]. The dynamics of a CO<sub>2</sub> laser with feedback requires a more detailed description than a simple three-dimensional (3D) flow for a quantitative comparison between numerical results and experimental measurements [6].

Within the large variety of class-B lasers, which also includes solid state and semiconductor lasers, diode-pumped Nd:YAG (yttrium aluminum garnet) lasers can be smaller than CO<sub>2</sub> lasers, with cavity lengths of a few centimeters or less, and may be designed to be more robust against environmental perturbations [7]. In this paper, we model the Nd:YAG laser with feedback by a set of three coupled differential equations, one each for the laser intensity, the population inversion, and the voltage of the feedback loop.

In the laser system we study either the pump parameter or cavity losses can be modulated at rates of several MHz. However, the decay rate of the electric field in the cavity is much faster than that of the population inversion. Loss modulation is therefore more effective at influencing the intensity dynamics of the laser than pump modulation. Compared with EOMs, acousto-optic modulators (AOMs) operating in the visible or near-infrared region offer the considerable advantages of (1) a driving voltage lower than that of EOMs, and (2) not requiring the use of intracavity polarization elements (Brewster windows, gratings, etc.). For this reason, the voltage of the feedback network will modulate the cavity loss via an AOM.

The dynamics of the Nd:YAG laser with feedback reveals the presence of two distinct regions of instability easily accessible by varying the bias voltage in the feedback loop. These regimes bound the domain where the stationary solution is stable. Toward positive bias, the transition to oscillatory behavior occurs through a subcritical Hopf bifurcation. Toward negative bias, the transition occurs through a supercritical Hopf bifurcation. Though the subcritical and supercritical bifurcations cannot be distinguished in the linearized model, the presence of hysteresis [8] in the numerical simu-

lation and in the laser system are good indications that the bifurcation at positive bias is subcritical.

As the transition to chaos in the experiment is very abrupt and leads quickly to high-amplitude chaos, we focus part of our attention on softening this transition to increase the variety of lower-amplitude chaotic dynamics available to the function generator. Control of chaos often takes advantage of steady states or periodic orbits inside a chaotic attractor to regularize dynamics. One of the major ways in which this is accomplished is by applying perturbations to state variables or system parameters. The key idea in the pioneering work by Ott, Grebogi, and Yorke (OGY) [9] is to use linear control theory and feedback on a system parameter to direct the motion of trajectories along the stable manifold of an unstable state. A scalar version of the OGY control method, occasional proportional feedback [10], and some variations of it have been successfully applied to stabilize unstable steady states and periodic orbits in a multimode Nd:YAG frequency-doubled laser (the green problem) [11–14].

The problem of the stabilization of an unstable steady state can also be approached by using a derivative control on a state variable, i.e., feedback control loops containing terms proportional to the derivative of the output of a given system. Derivative control has been successfully applied to many systems, for example Refs. [15–19], for stabilization. Other forms of control have also been used to maintain chaos, as in Ref. [20].

As we would prefer to use control for a purpose intermediate between suppressing and sustaining chaos, we look to employ the derivative control to alter the dynamics within the chaotic regions without eliminating the chaos.

The paper is organized as follows. Section II describes the design of the function generator. In Sec. III, we report on the experimental measurements of the laser dynamics with feedback as well as with control. We compare the probability distributions, power spectra, and leading Lyapunov exponents of the intensity wave forms that the laser generates for different values of the feedback bias. Section IV contains the theoretical model for the laser, and describes the results of linear stability analysis. Conclusions are drawn in Sec. V.

## II. EXPERIMENTAL APPARATUS

Our function generator is the diode-pumped solid state laser, including the feedback loop and an additional control loop, shown in Fig. 1. The crystal, Nd:YAG, has an absorption band centered near 810 nm, and lases near 1064 nm. One face of the crystal is coated with a dielectric mirror highly reflective at 1064 nm and highly transmissive at 810 nm. Population inversion in the solid-state laser is achieved by diode laser pumping at 810 nm through that face. The beam from the diode (SDL model 2350H1) is shaped and focused down to a small region inside the crystal.

The output coupler is a spherical mirror with a radius of curvature of 10 cm and a transmissivity  $T$  of 2% at 1064 nm. The optical length  $L$  of the cavity is approximately 9 cm. From these figures, the decay rate  $k_0$  for the laser intensity would be estimated as  $cT/2L = 3.3 \times 10^7 \text{ s}^{-1}$ , where  $c$  is the speed of light in vacuum. The cavity loss parameter must

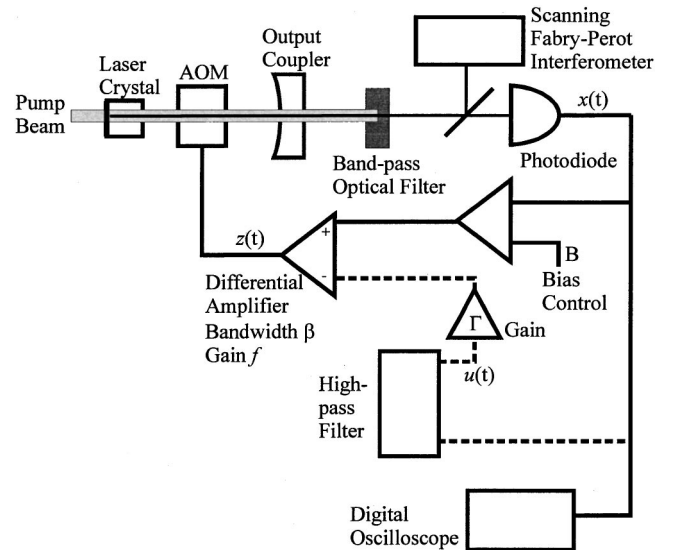


FIG. 1. Experimental setup of a diode-pumped Nd:YAG laser with an intracavity acousto-optic modulator and a feedback network. The solid line connecting the detector to the AOM indicates the main feedback loop generating the dynamics. The dashed line indicates the additional control loop including a reshaping filter, Wavetek model 452, in the high-pass configuration with a slope of 48 dB per octave. With or without the control loop being active, the bias  $B$  is a tuning parameter that allows access to a variety of laser dynamics.

also take into account diffraction losses, scattering losses, and insertion losses due to the AOM. From observation of the behavior of the experiment, a reasonable estimate of the net cavity loss is  $k_0 = 6.6 \times 10^7 \text{ s}^{-1}$ , which is the value used in the model (Sec. IV).

Measurements of the laser intensity are obtained with a photodiode. We block the pump beam from the photodiode by placing a 1064-nm bandpass filter between the laser and the photodiode. The cavity and crystal are aligned such that the YAG laser operates in the TEM<sub>00</sub> Gaussian transverse mode. The longitudinal mode structure of the YAG laser is monitored with a scanning confocal Fabry-Perot interferometer. The cavity typically lases in one to three longitudinal modes, with more than one longitudinal mode occurring most often for high values of bias. As the laser does not contain any strongly polarizing elements within the cavity, the laser field may consist of a single polarization or of two orthogonal polarizations.

Between the crystal and the output coupler, the intracavity AOM allows an electrical signal to deflect a portion of the lasing beam, and therefore increase the cavity loss. Acoustic waves with an amplitude proportional in intensity to a voltage applied at the input of the AOM driver create a phase grating through which the light in the cavity passes. With the AOM in place and the input to its driver grounded, the laser threshold is found to be at a pump power of 21 mW and the operating condition is 39 mW, making the pump parameter  $P = 1.85$  for the measurements reported here.

The cavity loss induced by the modulator is proportional to  $\sin^2(\pi V/V_{\text{mod}})$ , where  $V$  is the voltage applied to the modulation input of the AOM driver and  $V_{\text{mod}}$  is the satura-

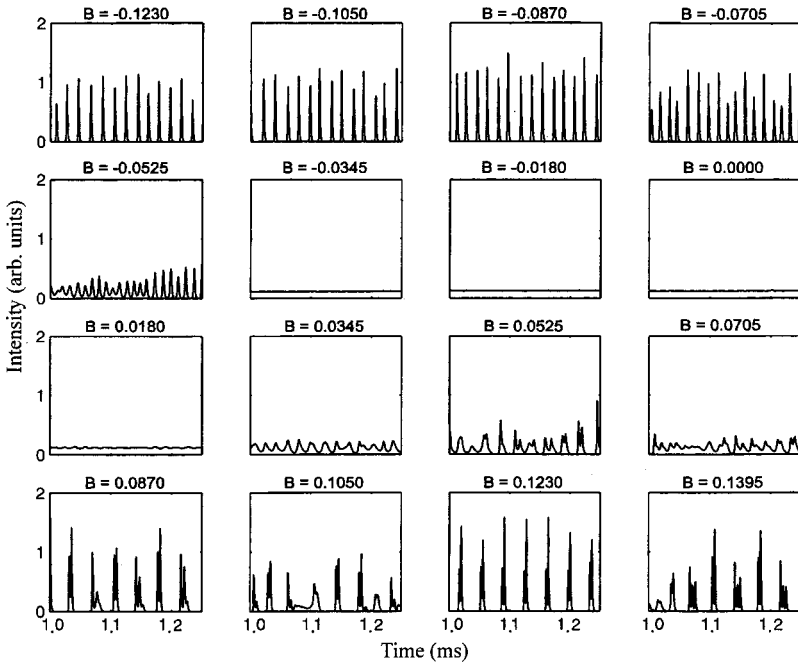


FIG. 2. Experimental time traces of the laser intensity with feedback but without the control loop for sixteen values of the bias  $B$ , showing chaotic spiking ( $B > -0.0525$  V), chaos just after the Hopf bifurcation ( $B = -0.0525$  V), near steady-state (cw) operation ( $B = -0.0345, -0.0180, 0.0000$ , and  $0.0180$  V), another variety of chaotic oscillations ( $B = 0.0345, 0.0525$ , and  $0.0705$  V), and bursting ( $B = 0.0870, 0.1050, 0.1230$ , and  $0.1395$  V).

tion voltage of the driver. With a dc signal applied to the AOM driver, the intensity output of the laser is stable and depends upon the cavity alignment and pump power.

Feedback can be added to the system by applying the voltage from the photodiode to the AOM driver through an amplifier/attenuator. Feedback with sufficient amplitude and bias destabilizes the steady state laser intensity value and gives rise to a variety of dynamical behaviors, including chaotic spiking and bursting.

We add a second branch of the feedback network, which we refer to as the control loop. This loop consists of a high-pass filter with a 48 dB per octave rolloff and an amplifier with adjustable gain  $\Gamma$ ; the output of this amplifier is applied to the inverting input of the differential amplifier in Fig. 1. This differential amplifier has a bandwidth  $\beta$  of 100 kHz. The net gain of the feedback loop is  $f$  and the net gain of the control loop is  $\Gamma f$ .

The delay of the feedback loop comes in two parts, propagation of the sound wave inside the AOM and transmission time of the electronic signal. The speed of sound within the AOM (a  $\text{PbMoO}_4$  crystal) is 3630 m/s and the distance between the transducer and the laser beam is approximately 5 mm. This corresponds to a time delay of  $1.37 \mu\text{s}$ . The time delay of the electronic portion of the loop, including the AOM driver, is measured to be approximately  $1.5 \mu\text{s}$ . The effect of the time delay on the dynamics is uncertain. However, we do not observe a peak in the power spectrum corresponding to the delay, which indicates that the effect is probably small. This is further confirmed by the fact that the characteristic frequency associated with the delay time is higher than the cutoff frequency of the feedback loop ( $f = 100$  kHz). The resulting dynamics occurs on the characteristic time of the laser relaxation oscillation frequency (about 75 kHz, see Sec. IV), which is about five times longer than that of the delay time. The effect of the time delay on the

dynamics will be systematically investigated in a future study.

Measurements of the photodiode signal are made with a digital oscilloscope (CompuScope CS1450) with 14 bits of precision and capable of acquiring 50 Msamples/s. We find measurement at 2 Msamples/s provides for sufficient resolution of the time series.

### III. EXPERIMENTAL RESULTS

Figure 2 shows short segments of experimental time traces seen by adjusting only the bias of the feedback loop without the effect of the second branch (control loop) shown in Fig. 1. These 16 values of the bias were chosen to illustrate a variety of intensity dynamics observed in the laser system. These dynamics include multiple-spike bursting at large positive bias, moderate-amplitude chaos at small negative and small positive bias, and high-amplitude chaotic spiking at large negative bias.

Table I displays the leading Lyapunov exponents calculated for the sets of data in Fig. 2. These calculations were performed with the software package CSPW2, which uses the algorithms described in Ref. [21]. When the intensity signal becomes nearly steady, the small amount of ambient noise recorded by the oscilloscope (0.02 peak-to-peak in the arbitrary units used in these figures) is registered by the CSPW package as a chaotic signal. For this reason, we never calculate a nonpositive leading Lyapunov exponent.

Figure 3 shows a bifurcation diagram of the laser dynamics with respect to the bias of the feedback loop, still without the additional control loop present. Each vertical strip in the diagram represents the discrete probability density function (PDF) of the laser intensity at a particular value of bias. The darkness at each location represents the relative amount of time the laser spends at a particular intensity. We have chosen to examine the PDF of the intensity signal because from

TABLE I. Leading Lyapunov exponents as calculated by the CSPW program for the time series used to generate Figs. 2, 4, and 5. When the laser is near steady-state operation ( $B = -0.0345, -0.0180, 0.0000, \text{ and } 0.0180$  V), noise in detection equipment results in calculation of what is most likely a false positive Lyapunov exponent.

Bias(V)	Leading Lyapunov ( $10^6 \text{ s}^{-1}$ )
-0.1230	2.12
-0.1050	2.06
-0.0870	2.00
-0.0705	1.70
-0.0525	0.28
-0.0345	2.34
-0.0180	2.88
0.0000	1.66
0.0180	0.88
0.0345	0.34
0.0525	0.96
0.0705	0.78
0.0870	2.30
0.1050	1.34
0.1230	1.86
0.1395	1.80

the PDF we can calculate the standard statistical measures. Arrows at the bottom of the figure indicate locations that have been sampled to create Figs. 2, 4, and 5.

In Fig. 4, we have plotted the normalized discrete probability density functions for the same values of bias as in Fig. 2. The slices of Fig. 3 allow us to distinguish between very different sorts of behaviors that appear similar in both the estimates of leading Lyapunov exponent and the bifurcation diagram of Fig. 3. Note, for example, the cusped tail in the PDF of the spiking behavior ( $B \leq -0.0705$  V), as opposed to

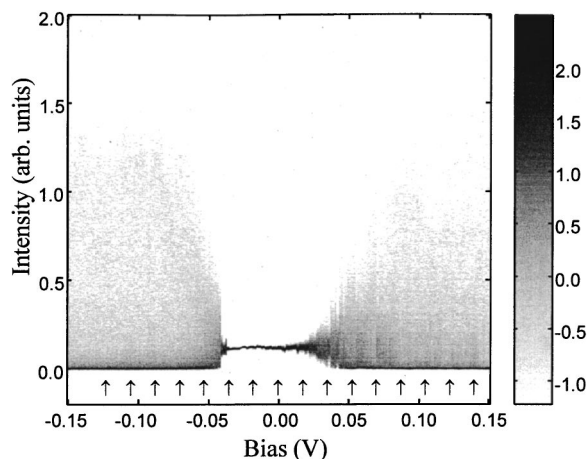


FIG. 3. Bifurcation diagram of the discrete probability distribution function (PDF) of the laser intensity signal for 200 values of feedback bias  $B$  without control. Arrows indicate the bias values at which the time traces in Fig. 2 were obtained. The grayscale axis represents the  $\log_{10}$  of the probability.

the more exponential tail in the PDF of the bursting ( $B \geq 0.0870$ ).

The power spectra of the dynamics at the same values of bias are displayed in Fig. 5. The main peak when the laser is near steady-state operation ( $B = -0.0345, -0.0180, \text{ and } 0.000$  V) represents the laser relaxation oscillation frequency.

Figure 6 shows a bifurcation diagram of the laser dynamics with the control loop being active. The control loop significantly alters the dynamics of the laser for all regions where the laser was not already in steady state. In the case of this diagram, the onset of chaos is significantly delayed in the direction of negative bias. For positive bias values, the regions of bursting are replaced by limit cycles or chaos, both with smaller amplitudes than in Fig. 2.

The effect of our filtering control on the time series is shown in Fig. 7, where we display excerpts of the traces of the laser intensity for the same 16 values of bias as in Fig. 2, but with the control loop being active. Note the expanded intensity scale. Table II shows the leading Lyapunov exponents calculated for these sets of data.

In Fig. 8, we present the PDFs calculated for these the wave forms produced with control at the same values of bias. The intensity scale has been expanded because the range of the laser intensity is smaller. Figure 9 displays the corresponding power spectra. Both PDFs and power spectra are markedly different than those found in Figs. 2–5.

The form of control explored in this section renders the transition from steady state to chaos to be more gradual. The control loop we have used to quench the dynamical range of the laser intensity has increased the variety of distinct behaviors that the laser intensity signal can exhibit.

In this section, we have been able to evoke a wide variety of chaotic wave forms from the laser. These wave forms can be distinguished from one another by their statistical characteristics and power spectra. In this sense, we have been able to record and classify the laser intensity dynamics. One can now view the laser as a device for selecting and generating chaotic wave forms with desired characteristics.

#### IV. MODEL AND NUMERICAL ANALYSIS

Let us consider the experimental apparatus shown in Fig. 1. Our goal in modeling the laser with feedback is to retain the coarse features of the laser intensity behavior. Such a system can be most simply described by three first-order differential equations, one each for the laser intensity  $I$ , the population inversion  $\Delta$ , and the modulation voltage  $V$  applied to the intracavity AOM:

$$\begin{aligned} \dot{I} &= -k_0 \left[ 1 + a \sin^2 \left( \frac{\pi V}{V_{\text{mod}}} \right) \right] I + g I \Delta, \\ \dot{\Delta} &= -\gamma \Delta - 2g I \Delta + \gamma \Delta_0, \\ \dot{V} &= -\beta (V - \tilde{B} - \tilde{f} I), \end{aligned} \quad (1)$$

where  $k_0$  is the cavity loss parameter introduced in Sec. II. The parameter  $a$  is the modulation strength of the additional losses introduced by the AOM modulation signal,  $\gamma$  is the population inversion decay rate,  $\beta$  is the damping rate of the feedback loop ( $2\pi$  times the cutoff frequency),  $g$  is the field-

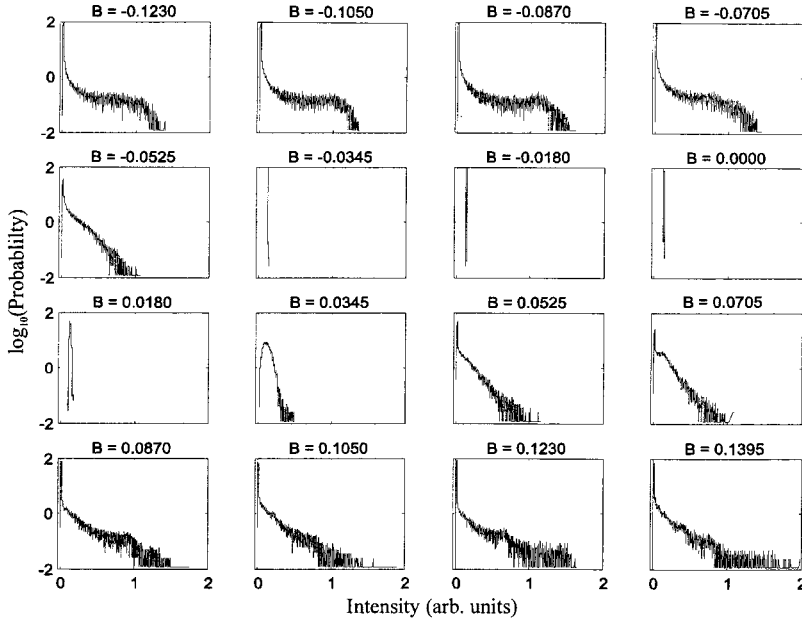


FIG. 4. PDFs taken from Fig. 3 for the same values of bias displayed in Fig. 2. A variety of shapes can be seen and the transition between them is also apparent. The area under each curve is normalized to 1 and the curves are displayed on a log-linear scale.

matter coupling constant,  $\tilde{f}$  is the scaling between intensity incident on the photodiode and the voltage read from it times the amplification of the differential amplifier, and  $\tilde{B}$  is a bias voltage applied to the modulator preamplifier. The parameter  $\Delta_0$  represents the population inversion induced by the action of the diode-pump beam.

With suitable normalization,  $P = \Delta_0 g / k_0$ ,  $f = \pi \tilde{f} \gamma / (2g V_{\text{mod}})$ ,  $B = \pi \tilde{B} / V_{\text{mod}}$ ,  $x = 2gI / \gamma$ ,  $y = g\Delta / k_0$ , and  $z = \pi V / V_{\text{mod}}$ , these equations become

$$\begin{aligned} \dot{x} &= -k_0 x [1 + a \sin^2(z) - y], \\ \dot{y} &= -\gamma (y - P + xy), \\ \dot{z} &= -\beta (z - B - fx). \end{aligned} \quad (2)$$

In this notation, the intensity  $x$  is normalized to the saturation intensity, the population inversion  $y$  and the pump  $P$  are normalized to the threshold population inversion, and the feedback  $z$  and bias  $B$  are normalized relative to the range of the modulation. For our model, we use the parameter values  $k_0 = 6.6 \times 10^7 \text{ s}^{-1}$ ,  $\gamma = 4.166 \times 10^3 \text{ s}^{-1}$ ,  $\beta = 6.28 \times 10^5 \text{ s}^{-1}$ ,  $a = 0.052$ ,  $P = 1.85$ , and  $f$  can be tuned between 0 and 1.

From Eqs. (2), we can show that the condition

$$\arcsin \left( \sqrt{\frac{P}{a(1+\bar{x})} - \frac{1}{a}} \right) - \bar{x}f - B = 0 \quad (3)$$

is fulfilled by the stationary solution of the model, denoted by the vector  $\bar{\mathbf{r}}(\bar{x}, \bar{y}, \bar{z})$ . Once the solutions of Eq. (3) are known, the stationary values of the other two variables are  $\bar{y} = P / (1 + \bar{x})$  and  $\bar{z} = B + \bar{x}f$ .

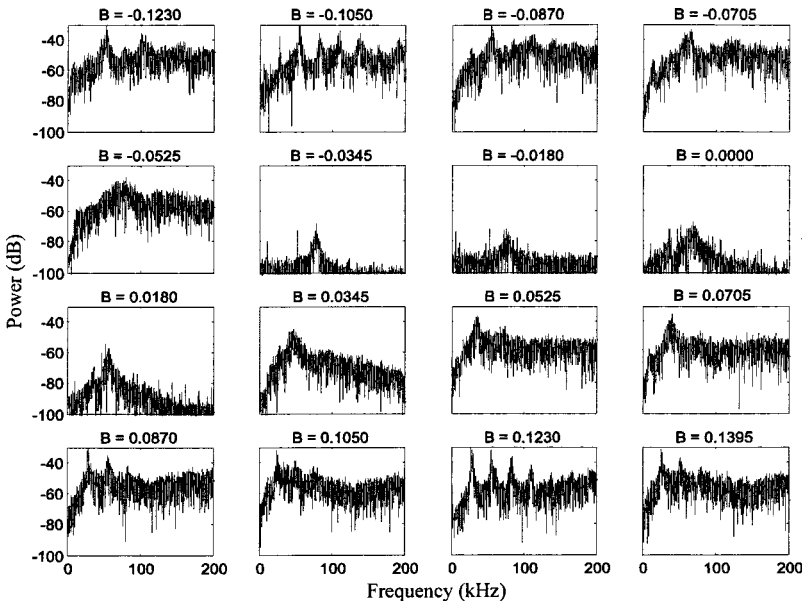


FIG. 5. Power spectra for the laser intensity signals of Fig. 2. The peaks observed near steady-state operation represent the characteristic laser relaxation oscillation frequency (approximately 79 kHz). Away from these values of bias, the laser exhibits a variety of broad spectral shapes.

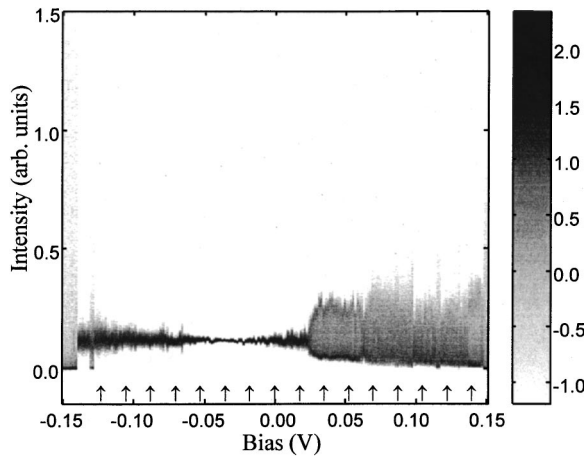


FIG. 6. Bifurcation diagram of the PDF of the laser intensity signal for 200 values of bias with the control loop active. The controlling filter rolloff frequency  $\omega = 5$  kHz and the gain  $\Gamma$  have been tuned to produce the largest window of steady-state operation. Arrows indicate the bias values for which the time traces, PDFs, and power spectra are taken in Figs. 7, 8, and 9. The grayscale axis represents the  $\log_{10}$  of the probability.

When the laser without feedback is perturbed away from equilibrium, it will display relaxation oscillations at the frequency given by

$$f_{\text{Rel}} = \frac{\sqrt{\gamma k_0 (P - 1)}}{2\pi}. \quad (4)$$

This frequency also gives the characteristic time scale of the laser dynamics, which in our case is about  $13\mu\text{s}$ .

In order to determine the stability of an equilibrium solution  $\bar{\mathbf{r}}$  of Eqs. (2), we consider the Jacobian matrix  $\mathbf{Df}(\mathbf{r})$  of the partial derivatives evaluated at  $\bar{\mathbf{r}}$ . Stability of  $\bar{\mathbf{r}}$  in the face of a small perturbation is determined by the eigenvalues of

TABLE II. Leading Lyapunov exponents calculated for the laser with feedback and control at the same bias values as in Fig. 7. Again, it is likely that the calculated values for dynamics near steady state are false positives.

Bias(V)	Leading Lyapunov Exponent ( $10^6 \text{ s}^{-1}$ )
-0.1230	0.38
-0.1050	0.50
-0.0870	0.82
-0.0705	1.06
-0.0525	1.92
-0.0345	2.10
-0.1800	2.36
0.0000	1.08
0.0180	0.52
0.0345	0.30
0.0525	0.24
0.0705	0.14
0.0870	0.20
0.1050	0.16
0.1230	0.14
0.1395	0.28

the linearized flow represented by  $\dot{\mathbf{v}} = \mathbf{Df}(\bar{\mathbf{r}})\mathbf{v}$ , where the vector  $\mathbf{v}$  denotes a small deviation from the fixed point. The real parts of the three eigenvalues are reported in Fig. 10. Note that the leading eigenvalue, where positive, is of the order of  $10^6 \text{ s}^{-1}$ , as are the leading Lyapunov exponents calculated for the experiment in Table I. The values of the bias  $B$ , where the fixed point is unstable, occur where the real part of any eigenvalue is positive. In our case, the fixed point undergoes a Hopf bifurcation where an eigenvalue intersects the zero line in Fig. 10. The imaginary part of this eigenvalue corresponds to a frequency of 76 kHz, comparable with the relax-

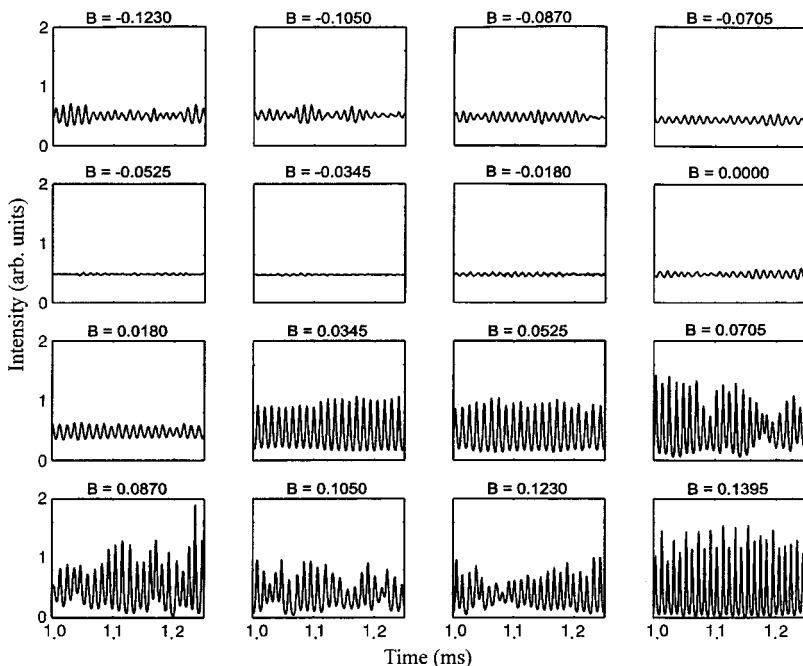


FIG. 7. Selected time traces of the laser intensity with control for 16 values of the bias  $B$ , showing chaotic oscillations ( $B \leq -0.1050$  V), near-periodic behavior ( $B = -0.0870, -0.0705, 0.0000, 0.0180, 0.0345, \text{ and } 0.0525$  V), near-steady-state (cw) operation ( $B = -0.0525, -0.0345, \text{ and } -0.0180$  V), and chaotic spiking ( $B \geq 0.0705$  V).

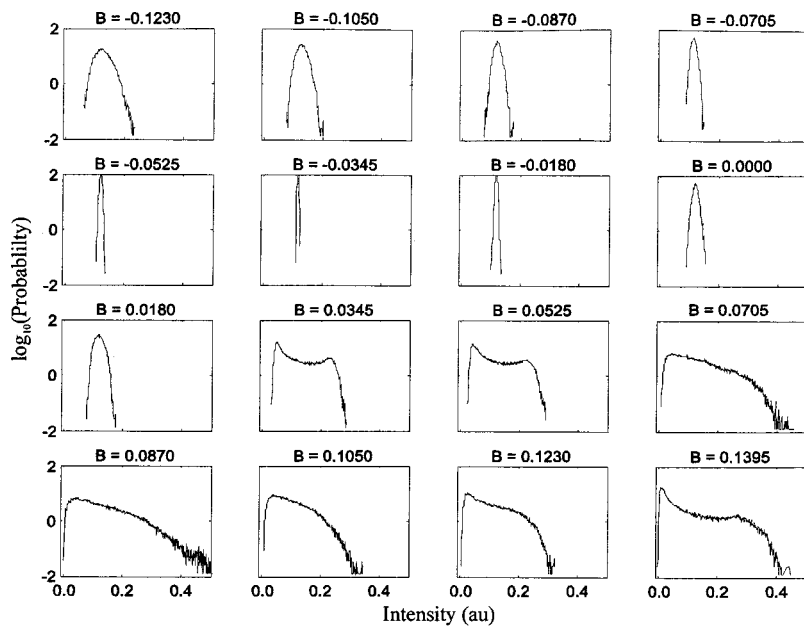


FIG. 8. PDFs for the same values of bias as in Fig. 7. A variety of shapes distinct from those in Fig. 4 are evident for large negative and positive bias values.

ation oscillation frequency of 76.9 kHz given by Eq. (4).

The bifurcation diagram for the model system is shown in Fig. 11. The model parameter  $B$ , corresponding to the feedback bias, is slowly increased from negative to positive in a time of 0.05 s, considerably longer than the microsecond time scale of the laser dynamics. On the vertical axis, the local maxima and minima of the laser intensity are shown. Toward negative bias, there is evidence of a cascade of subharmonic bifurcations ending with chaos after a supercritical Hopf bifurcation. However, the model does not display bursting for positive bias and the spiking at large negative bias becomes regular in amplitude rather than chaotic as in the experimental system. The model is also much more sensitive to the choice of parameters  $P$ ,  $a$ , and  $f$  than the laser system.

For positive values of  $B$ , the transition to a region of large amplitude oscillations occurs through a subcritical Hopf bi-

furcation ( $B = 1.05$ ). This bifurcation exhibits hysteresis as the control parameter is varied in the opposite direction ( $B = 0.89$ ). The model does not display the chaotic bursting evident in the experiment.

If we denote the input signal proportional to the laser intensity by  $x(t)$ , the output signal  $u(t)$  of an RC first-order filter is given by the differential equation  $\dot{u} = -\omega u + \dot{x}$ , where  $\omega$  is defined as  $2\pi$  times the rolloff frequency ( $\omega = 1/RC$ ). In our model, we insert this perturbation into the feedback loop by adding a term to the equation governing  $z(t)$ . With a gain factor  $\Gamma$ , the perturbation signal affects the dynamics in following way:

$$\dot{x} = -k_0 x [1 + a \sin^2(z) - y], \tag{5}$$

$$\dot{y} = -\gamma(y - P + xy),$$

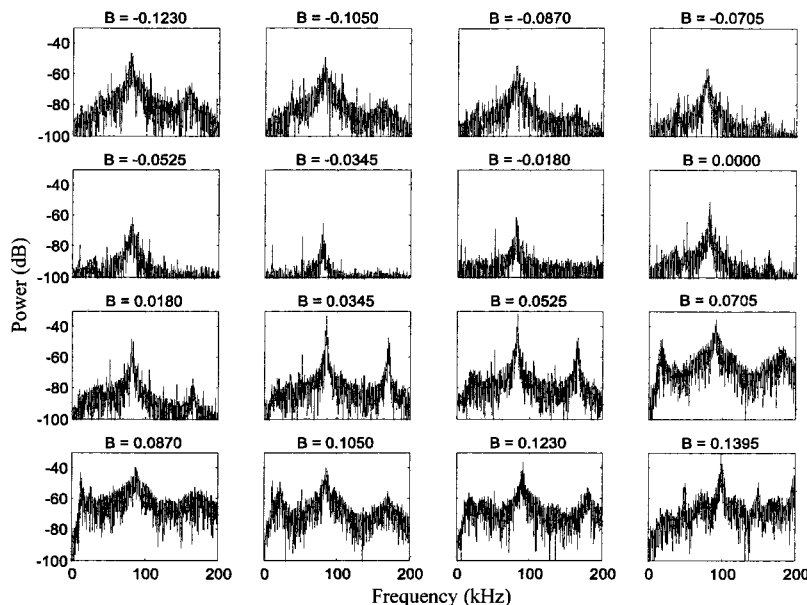


FIG. 9. Power spectra for the laser intensity signals shown in Fig. 7. The peaks observed near steady-state operation again represent the laser relaxation oscillation frequency. Away from these values of bias, the spectral characteristics of the laser signal differ significantly from those in Fig. 5.

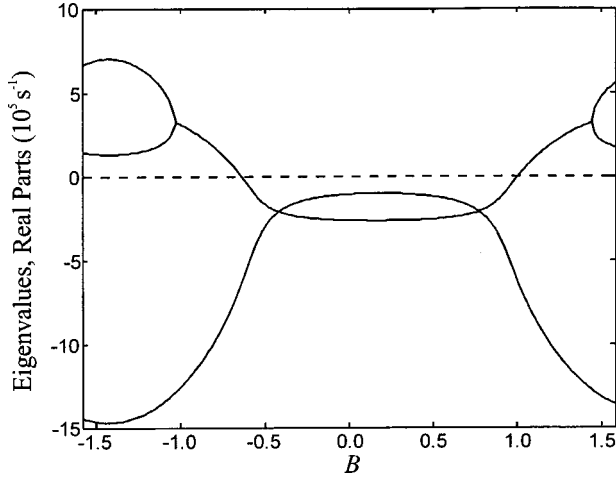


FIG. 10. Plots of the real parts of the eigenvalues of the Jacobian matrix associated with Eqs. (2) as a function of the tuning parameter  $B$ . The parameter values are  $a=0.052$ ,  $k_0=6.6\times 10^7\text{ s}^{-1}$ ,  $\gamma=4.166\times 10^4\text{ s}^{-1}$ ,  $P=1.85$ ,  $\beta=6.28\times 10^5\text{ rad/s}$ , and  $f=0.75$ . The leading eigenvalue, where positive, is of the order of  $10^6\text{ s}^{-1}$ , comparable to the Lyapunov exponents calculated in Table I.

$$\dot{z} = -\beta[z - B - f(x - \Gamma u)],$$

$$\dot{u} = \dot{x} - \omega u.$$

It is always possible to find a region in the parameter space  $(\omega, \Gamma)$  where the control in Eq. (5) stabilizes the steady state for a given value of  $B$ . But a value of  $\omega$  near to or lower than the leading frequency component of the laser intensity fluctuations may significantly alter the system dynamics without stabilizing the steady state. In our case, this leading frequency corresponds to the frequency of the limit cycle just after the Hopf bifurcation.

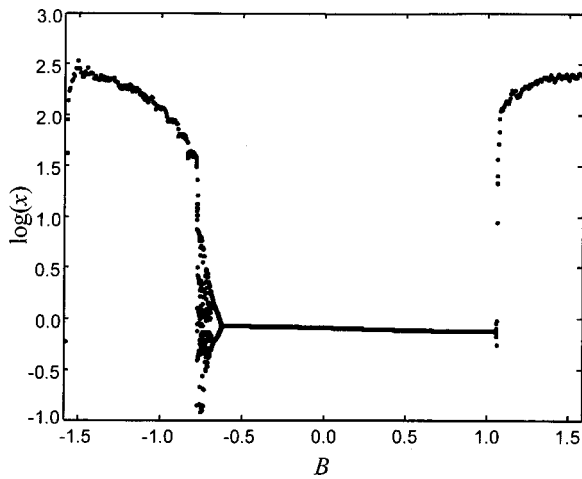


FIG. 11. Bifurcation diagram of the local maxima and minima of the laser intensity vs  $B$ . The parameter values are the same as those in Fig. 10. The scan time is 0.05 s, and the steady-state value is displayed where it is stable. The period doubling cascade begins around  $B = -0.64$ .

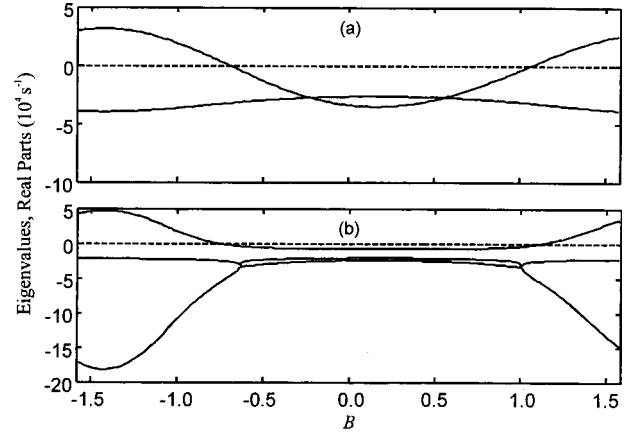


FIG. 12. (a) Real parts of the eigenvalues of the controlled system of Eqs. (5) (first-order filter) vs  $B$ . (b) Real parts of the eigenvalues of the controlled system of Eqs. (6) (third-order filter) vs  $B$ . The parameters of the control loop are  $\omega=5\text{ kHz}$  and  $g=0.88$ . The magnitude of the leading eigenvalue is reduced in both cases by a factor of 10 from that calculated for the model with feedback only.

In the experiment in Sec. III, we use a higher-order filter to render the process more selective in frequency. Such a selective filter control can be modeled by cascading several first-order filters. Here, we limit the analysis to a third-order filter. The overall dynamics is now described by the following system of differential equations:

$$\dot{x} = -k_0 x [1 + a \sin^2(z) - y],$$

$$\dot{y} = -\gamma(y - P + xy),$$

$$\dot{z} = -\beta[z - B - f(x - \Gamma u_3)],$$

$$\dot{u}_1 = \dot{x} - \omega u_1,$$

$$\dot{u}_2 = \dot{u}_1 - \omega u_2,$$

$$\dot{u}_3 = \dot{u}_2 - \omega u_3. \quad (6)$$

The results of the linear stability analysis for both model systems from Eqs. (5) and (6) are reported in Figs. 12(a) and 12(b), respectively, with the most negative exponent not displayed in both cases. Both first- and third-order filters reduce the range of the magnitude of the leading eigenvalue.

The global effect of the controlling perturbation on the simulated laser dynamics, as seen in the bifurcation diagram in Fig. 13, shows the enlargement of the stability domain of the controlled dynamics. The chaotic region after the supercritical Hopf bifurcation is replaced by the stationary solution. The subcritical Hopf bifurcation at positive  $B$  is now replaced by a supercritical Hopf bifurcation.

Comparison of the power spectra and time-delay embeddings for theoretical and experimental results are displayed in Fig. 14. We present the chaotic attractor just after the onset of chaos (after the Hopf bifurcation) to compare it with the model. The leading frequency in the numerical simulation is roughly 75 kHz compared to about 83 kHz in the experiment. Both peaks are near the relaxation oscillation fre-

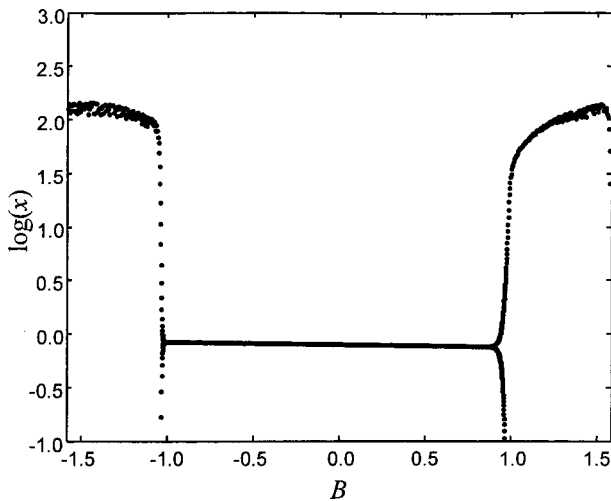


FIG. 13. Bifurcation diagram of the local maxima and minima of the laser intensity vs  $B$  for the controlled dynamics of Eqs. (6). The laser model parameter values are the same as those in Fig. 11. The scan time is 0.05 s and again the steady-state value is displayed where it is stable. The parameters of the control loop are  $\omega = 5$  kHz and  $g = 0.88$ . The supercritical bifurcation at negative  $B$  now begins near  $B = -0.96$ .

quency of the laser and, as a consequence, the Hopf frequency. In both spectra, subharmonic peaks are observed at approximately one-third the frequency of the main peak.

## V. CONCLUSION

Until recently, typical laser applications have focused on either steady-state operation or regularly pulsed operation. In this paper, the dynamics of an Nd:YAG laser subject to feedback modulation of the intracavity losses via an AOM have been explored. Tuning the bias of the feedback loop allows easy exploration of a range of intensity dynamics that includes a sudden transition from steady state to high-amplitude spiking and bursting. An additional branch of the feedback loop that suppresses higher-frequency components of the feedback alters the dynamics of the laser while preserving the chaos. With this controlling loop active, the transition to chaos is more gradual and low-amplitude chaotic oscillations are observed.

We have demonstrated that a laser with suitably designed

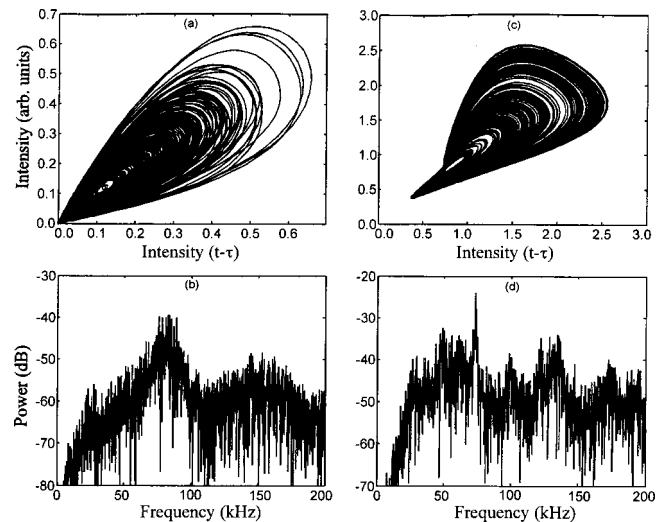


FIG. 14. Left side shows power spectra and attractor reconstructed from the intensity series of the experiment (with feedback only) at a bias of  $-0.045$  V and with embedding time delay  $\tau = 0.8$   $\mu$ s. Right side shows power spectra and attractor reconstructed from the  $x$  values of the simulation of Eqs. (2) (also with feedback only) at  $B = -0.711$  with embedding time delay  $\tau = 0.8$   $\mu$ s.

feedback can serve as a tunable generator of chaotic “functions.” These wave forms can be characterized through bifurcation diagrams that record discrete probability density functions, power spectra or other measures of the dynamics. Bifurcation diagrams can then be used as libraries or lookup tables to select particular chaotic signals by their statistical characteristics.

## ACKNOWLEDGMENTS

This research was supported in part by the U.S. Department of Energy, Office of Basic Energy Sciences. The Oak Ridge National Laboratory is managed for the U.S. DOE by UT-Battelle, LLC, under Contract No. DE-AC05-00OR22725. We also gratefully acknowledge support from the Office of Naval Research (Physics). R.M. also wishes to acknowledge European Contract No. HPRN-CT-2000-00158 for supporting his visit to the University of Maryland. We thank Yuri Braiman for helpful discussions and Don Martin for expert technical assistance.

- [1] H. Haken, *Light* (Elsevier Science, New York, 1985), Vol. 2, p. 189.
- [2] *Instabilities and Chaos in Quantum Optics*, edited by F. T. Arecchi and R. G. Harrison (Springer, Berlin, 1987).
- [3] O. Svelto, *Principles of Lasers* (Plenum, New York, 1982), p. 203.
- [4] P. Colet and R. Roy, *Opt. Lett.* **19**, 2056 (1994); G. D. Van Wiggeren and R. Roy, *Science* **279**, 1198 (1998); *Phys. Rev. Lett.* **81**, 3547 (1998).
- [5] F. T. Arecchi, W. Gadomski, and R. Meucci, *Phys. Rev. A* **34**, 1617 (1986).
- [6] A. Varone, A. Politi, and M. Ciofini, *Phys. Rev. A* **52**, 3176 (1995).
- [7] W. Koechner, *Solid-State Laser Engineering*, 5th ed. (Springer-Verlag, Berlin, 1999).
- [8] S. H. Strogatz, *Nonlinear Dynamics and Chaos* (Addison-Wesley, Reading, MA, 1995), pp. 252–253.
- [9] E. Ott, C. Grebogi, and J. A. Yorke, *Phys. Rev. Lett.* **64**, 1196 (1990); T. Shimobrot, C. Grebogi, E. Ott, and J. A. Yorke, *Nature* (London) **363**, 411 (1993).
- [10] E. H. Hunt, *Phys. Rev. Lett.* **67**, 1953 (1992).
- [11] R. Roy *et al.*, *Phys. Rev. Lett.* **68**, 1259 (1992).

- [12] Z. Gills *et al.*, Phys. Rev. Lett. **69**, 3169 (1992).
- [13] T. W. Carr and I. B. Schwartz, Phys. Rev. E **51**, 5109 (1995).
- [14] P. Colet, R. Roy, and K. Weisenfeld, Phys. Rev. E **50**, 3453 (1996).
- [15] G. A. Johnson and E. R. Hunt, IEEE Trans. Circuits Syst., I: Fundam. Theory Appl. **40**, 833 (1993).
- [16] P. Parmananda *et al.*, Phys. Rev. E **49**, 5007 (1994).
- [17] A. Namajunas, K. Pyragas, and A. Tamasevicius, Phys. Lett. A **204**, 255 (1995); Int. J. Bifurcation Chaos Appl. Sci. Eng. **7**, 957 (1997).
- [18] S. Bielawski, M. Bouazaoui, D. Derozier, and P. Glorieux, Phys. Rev. E **47**, 3276 (1993).
- [19] M. Ciofini, A. Labate, R. Meucci, and M. Galanti, Phys. Rev. E **60**, 398 (1999).
- [20] I. Triandaf and I. B. Schwartz, Phys. Rev. E **62**, 3529 (2000); I. Visarath *et al.*, Chaos **7**, 605 (1997).
- [21] H. D. I. Abarbanel, *Analysis of Observed Chaotic Data* (Springer-Verlag, New York, 1996).